CHINESE OPTICS LETTERS

Vol. 22, No. 2 | February 2024

2.32 W anti-misaligned Er:LuAG single-longitudinal-mode laser in the double corner-cube-retroreflector resonator and MOPA system

Jiawei Fan (范佳玮)[1], Youlun Ju (鞠有伦)[1], Chenchen Jiang (姜辰晨)[1], Yue Yuan (袁 越)[2], Dong Yan (闫 东)[1], Xingbang Yang (杨星帮)[1], Xiaoming Duan (段小明)[1,3], Tongyu Dai (戴通宇)[1*], Baoquan Yao (姚宝权)[1], and Jiaze Wu (吴佳泽)[1**]

[1] National Key Laboratory of Tunable Laser Technology, Harbin Institute of Technology, Harbin 150001, China

[2] Department of Physics and Chemistry, PLA Army Academy of Special Operations, Guangzhou 510507, China

[3] Zhengzhou Research Institute of Harbin Institute of Technology, Zhengzhou 450000, China

*Corresponding author: daitongyu2006@126.com

**Corresponding author: wujiaze@hit.edu.cn

Received September 2, 2023 | Accepted October 9, 2023 | Posted Online February 21, 2024

We demonstrate a high power, Er:LuAG single-longitudinal-mode laser in an anti-misaligned resonator. Based on the Faraday effect, a 1.61 W single-longitudinal-mode (SLM) laser is obtained with the double corner-cube-retroreflector (CCR) structure, and the tunable wavelength is 1649.2–1650.3 nm. Additionally, we investigate the anti-misalignment characteristics when the CCR moves and rotates along the optical axis. Furthermore, by utilizing the Er:LuAG amplifier, the maximum 2.32 W single-longitudinal-mode laser at 1649.6 nm is achieved. The beam quality factors M^2 of the 2.32 W Er:LuAG single-longitudinal-mode laser are 1.23 and 1.25 along the horizontal (x) and vertical (y) directions, respectively.

Keywords: Er:LuAG single-longitudinal-mode laser; Faraday effect; MOPA system; double corner-cube-retroreflector resonator.

DOI: 10.3788/COL202422.021401

1. Introduction

The applications of the all-solid-state single-longitudinal-mode laser aimed at a 1.6 μm eye-safe waveband are mainly focused on the coherent Doppler wind LIDAR[1–3], coherent imaging systems[4], and so on. Recently, many methods have been used to achieve the 1.6 μm single-longitudinal-mode (SLM) lasers with Er:YAG crystal, such as the twisted-mode cavity[5], the non-planar ring oscillator (NPRO)[6], the unidirectional operation of the ring cavity[7,8], and the intracavity Fabry–Perot etalons[9,10]. Among them, adopting the Faraday effect to obtain the SLM laser is the most effective and convenient.

In the applications of wind LIDAR, it is necessary to avoid the absorption peak of the gases for increasing the propagation distances. However, the main emission wavelength (1645 nm) of the Er:YAG crystal locates at the absorption peak of the CH_4, which greatly limits the detection range in the atmosphere. In comparison, another emission wavelength (1617 nm) is far away from the atmospheric absorption lines and more suitable for the wind LIDAR. In 2014, Deng *et al.* reported a 78.5 mW, 1617.6 nm Er:YAG SLM laser with three inserted etalons pumped by a laser diode[11]. In 2015, Yao *et al.* demonstrated the 130 mW SLM laser at 1617.2 nm based on the twisted-mode technique[5]. However, it is more difficult to generate the 1617 nm laser because the population inversion needed to form 1617 nm is more than for 1645 nm. In general, the 1645 nm laser is more inclined to oscillate and depletes the population inversion, thus suppressing the generation of 1617 nm laser.

To solve this problem, using the Er:LuAG crystal is more advantageous than using the Er:YAG. The main emission peak of Er:LuAG laser is around 1650 nm, and its absorption of CH_4 is lower than that of the Er:YAG. Moreover, LuAG has more favorable physical characteristics, such as better thermal conductivity and a higher melting point. More importantly, the Er:LuAG crystal has a relatively larger emission cross section at 1.6 μm (0.87×10^{-20} cm^2 for Er:LuAG vs. 0.55×10^{-20} cm^2 for Er:YAG) and absorption cross section around 1.5 μm than the Er:YAG (2.2×10^{-20} cm^2 for Er:LuAG vs. 1.22×10^{-20} cm^2 for Er:YAG). Therefore, the Er:LuAG has excellent application prospects in the Doppler LIDAR owing to the above advantages. So far, relatively few results have been reported on the Er:LuAG lasers, mainly focusing on continuous-wave (CW),

Q-switched[12–14], and SLM operation. For the SLM operation, the maximum output power was achieved in Ref. [15]. In 2015, Dai *et al.* first reported a 1650.2 nm Er:LuAG SLM laser with intracavity etalons. At the pump power of 9.18 W, the maximum SLM power was only 153 mW, corresponding to a slope efficiency of 4.3%[15].

In addition, improving the stability of the high-power SLM laser in poor environments is also essential. Over the past years, the retroreflectors (including the corner-cube-retroreflector and the cat-eye optical arrangement) have been widely reported due to its anti-misalignment characteristics[16–20]. Compared to the cat-eye arrangement, the corner-cube-retroreflector (CCR) has geometrically simple optical devices with fascinating optical properties for the ring cavity. Therefore, it is necessary to establish an Er:LuAG SLM laser in the CCR cavity to realize the optimum anti-misalignment performances in engineering applications.

In this paper, the maximum 2.32 W SLM Er:LuAG laser is obtained at 1649.6 nm by using the master-oscillator power-amplifier (MOPA) system, which is 15 times the reported SLM power at present. The Er:LuAG oscillator, based on the Faraday effect, realizes the SLM operation. We obtain an SLM Er:LuAG laser with a 1.61 W maximum power, wavelength tuning range of about 1.1 nm, and a slope efficiency of 15.18%. In addition, combined with the double CCR structures, the anti-misalignment features of the ring cavity have been further improved. The SLM power is then further increased with the MOPA system. At the seed power of 1.61 W, the SLM power at 1649.6 nm has reached 2.32 W via the amplifier. Reducing the injected power to 295 mW, achieves a maximum gain of 2.56 dB. In addition, under the SLM power of 2.32 W, M^2 factors of 1.23 and 1.25 in the horizontal (x) and vertical (y) directions are measured with a 90/10 knife-edge method[21].

2. Experimental Setup

The high-power, tunable Er:LuAG laser is mainly composed of an Er:LuAG SLM oscillator and a MOPA system, as shown in Fig. 1. In Fig. 1, the blue solid line shows the path of the pump laser, the red line shows the path of the oscillator laser, and the blue dotted line shows the path of the unabsorbed remaining pump laser.

The Er:LuAG SLM oscillator, with a total length of approximately 800 mm, is composed of CCR1 and CCR2 (with a diameter of 40 mm and height of 35 mm), an Er:LuAG gain medium, two output mirrors, P1 and P2 (polarizers), the Faraday rotator (a ferromagnetic crystal, which is surrounded by strong permanent magnets with a rotation angle of 45° independent of the input angle), a $\lambda/4$ plate, a plano-convex lens f3, and a Fabry–Perot etalon. To improve the anti-misalignment of the Er:LuAG SLM oscillator, the double CCRs have been introduced to ensure that the oscillating optical path will not change significantly when the CCR rotates or moves laterally[22]. The Er:LuAG SLM oscillator is pumped by a homemade Er/Yb fiber laser, which has a total power of 50 W with a beam quality of about 1.3. Figure 2 shows the wavelength of the Er/Yb fiber laser and the absorption cross section of the Er:LuAG crystal together[14]. It is obvious that the central wavelength of the pump laser is 1531.96 nm, close to the absorption peak of the Er:LuAG crystal.

Additionally, we have also measured the absorptivity of the Er:LuAG crystal under the different pump powers (the inset of Fig. 2), and the results show that the single-pass absorptivity is 57.5% when the pump power increases to 27.3 W. The pump light is shaped by the f1 and f2 lenses (10 mm and 200 mm, respectively) and reflected by M1. It is then focused to the center of the Er:LuAG crystal with a waist radius of 460 μm. The 0.5% (atomic fraction) doped Er:LuAG crystal with a length of 50 mm and a cross-sectional dimension of 1.7 mm × 5.5 mm is selected as the gain medium, which is installed in a water-cooled copper radiator at a temperature of 288 K. The P1 and P2 polarizers are both coated with highly reflective films for pumping light and pumping the 1.6 μm vertically polarized laser, which is highly transmissive for the 1.6 μm horizontally polarized laser. In addition, P1 and P2 can also be used as the output mirrors of the cavity. To realize the SLM laser, the combination of the

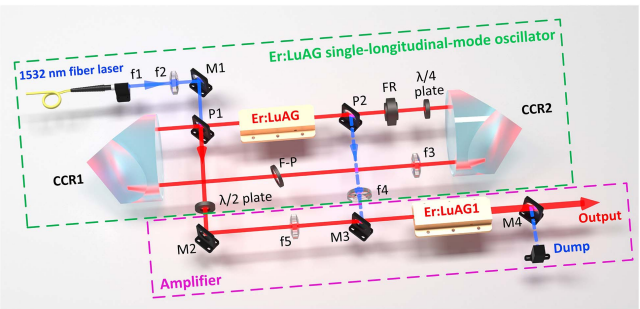

Fig. 1. Schematic diagram of the Er:LuAG SLM oscillator and the MOPA system. FR, Faraday rotator; F-P, Fabry-Perot etalon.

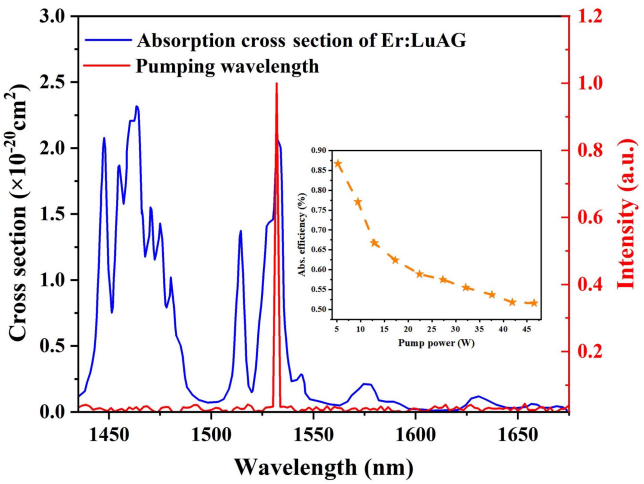

Fig. 2. Absorption cross section of the Er:LuAG crystal and the wavelength of the pump laser. Inset: the absorptivity of the Er:LuAG crystal under different pump powers.

Faraday rotator and the $\lambda/4$ plate makes the ring cavity operate unidirectionally, eliminating the spatial hole-burning effect. Additionally, an f3 lens with a focal length of 160 mm is placed in the symmetric position of the Er:LuAG crystal for improving the stability of the resonator. Finally, the SLM laser wavelength can be tuned by an uncoated 0.05 mm Fabry–Perot etalon.

The ABCD matrix has been used to analyze the stability of the Er:LuAG SLM oscillator with the double CCR structures[23]. In Fig. 3, the values of $(A + D)/2$ of the Er:LuAG SLM resonator and the oscillating spots under the different thermal focal lengths of the Er:LuAG have been calculated. As shown in Fig. 3(a), the resonator is stable when the thermal focal length is less than 190 mm. In Fig. 3(b), under the Er:LuAG thermal focal length of 140 mm, 160 mm, and 180 mm, the oscillating beam radii of the components in the double CCRs resonator have been simulated. The beam radius at the center of the Er:LuAG crystal is about 0.45 mm under the thermal focal length of 160 mm, which matches with the pump spot (460 μm). The beam radius of the Faraday rotator is approximately 0.30 mm, and the beam radius of the compensating f3 lens is about 0.46 mm at the 160 mm thermal focal length.

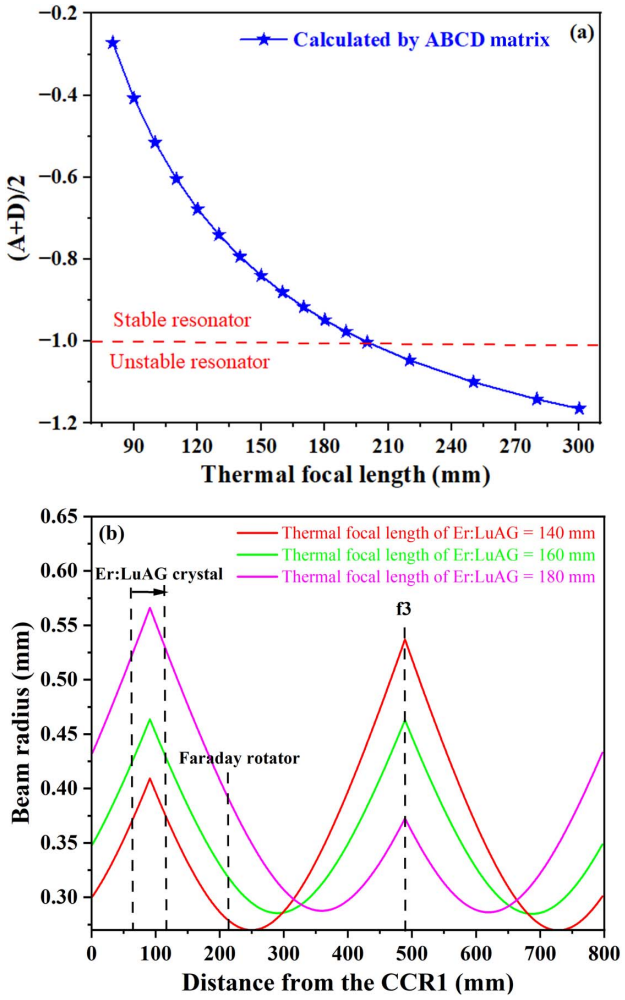

Fig. 3. (a) Value of $(A + D)/2$ versus the thermal focal length of the Er:LuAG crystal. (b) Oscillating spot in the double CCRs Er:LuAG oscillator under different thermal focal lengths.

3. Discussions and Results

First, we investigated the output characteristics of the Er:LuAG oscillator in the multi-longitudinal-mode (without the Faraday rotator). In this condition, the Er:LuAG oscillator outputs light from polarizers P1 and P2, which is vertically polarized in both directions. The total output power of the Er:LuAG oscillator increases linearly as the pump power increases, as shown in Fig. 4. The pump threshold is 22.4 W, and the maximum output power is 5.24 W at the pump power of 42.5 W with a slope efficiency of 20.07%. The laser is multimode (Fig. 4 inset), tested through a scanning Fabry–Perot interferometer with a free spectral range (FSR) of 1.5 GHz.

Then, by inserting the Faraday rotator into the cavity, the resonator can operate unidirectionally by adjusting the angle of the $\lambda/4$ plate in Fig. 1. The resonator has been changed to a traveling-wave cavity, eliminating the spatial hole burning effect by adding the isolation device and thus realizing the SLM operation.

As shown in Fig. 5(a), the maximum 1.61 W SLM laser at the pump power of 27.3 W has been obtained, corresponding to the slope efficiency of 15.18%. Furthermore, the maximum SLM power is limited by the Faraday rotator's damage threshold (92.3 W/cm^2). In addition, the unabsorbed remaining pump laser by the Er:LuAG crystal is used to pump the Er:LuAG amplifier, as shown in Fig. 1. In Fig. 5(b), the laser operates at the SLM measured by the Fabry–Perot interferometer (with an FSR of 1.5 GHz and a fineness of 1500), and the linewidth of the SLM Er:LuAG laser is less than 10.95 MHz according to the correspondence between the laser frequency and the scanning time. The wavelength of the SLM laser is 1649.6 nm,

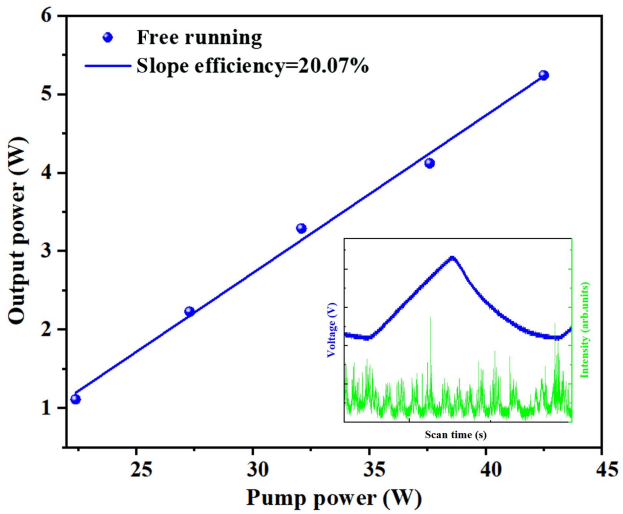

Fig. 4. Output power of the Er:LuAG oscillator without the Faraday rotator. Inset: Fabry–Perot spectrum.

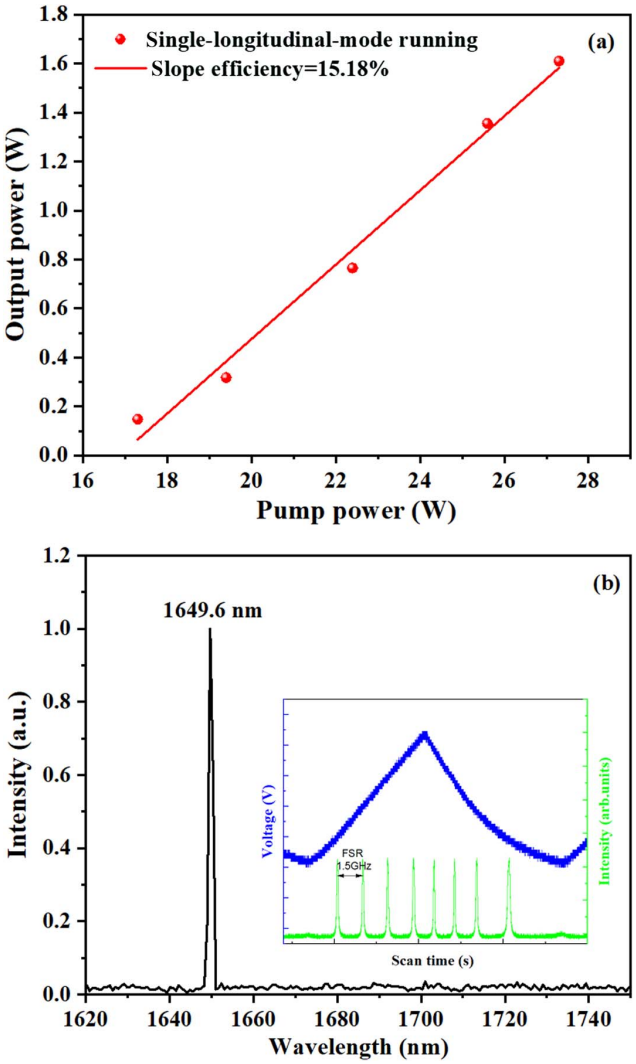

Fig. 5. Output characteristics of the Er:LuAG SLM oscillator. (a) The output power. (b) The output wavelength and the Fabry-Perot spectrum.

measured by the wavelength meter (Bristol 721A). In addition, the output laser is vertically polarized, as measured by the Glan prism.

Then, adopting a high-precision translation table fixed on the CCR2, we investigated the effects of moving (perpendicular and parallel to the CCR line directions) and rotating the CCR2 on the SLM power. Figure 6(a) indicates that with the increasing lateral displacements (perpendicular to the CCR direction), the resonator still has SLM laser output, despite a decrease in power. When the lateral displacement exceeds 0.1 mm, the output power has decreased to 50%. The above results indicate that the double CCRs resonator can offset the effect of the lateral displacement on the output power to some extent. In addition, the influence of the CCR horizontal displacements (parallel to the CCR direction) on the Er:LuAG SLM power has also been measured experimentally. By moving the CCR2, as shown in Fig. 6(b), the SLM power has been reduced to zero at a maximum translation distance of 5.5 mm. In addition, the effect of rotating the CCR2

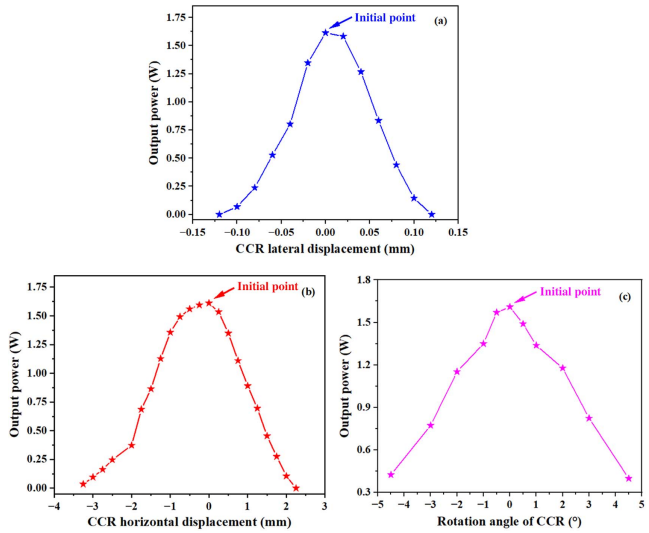

Fig. 6. Influence of the CCR on the Er:LuAG SLM power. (a) Perpendicular to the CCR direction. (b) Parallel to the CCR line. (c) Rotating along the point on the axis.

along the axis on the power of the Er:LuAG SLM laser has also been analyzed. When the maximum rotation angle is 9°, as shown in Fig. 6(c), the power has reduced to 0. The above experimental results indicate that the SLM power is not sensitive to the changes in the movement distances and rotation angles of the CCR2. As a result, the double CCRs structure is useful for improving the stability of the Er:LuAG SLM laser, and the anti-misalignment abilities of the Er:LuAG laser can also be greatly improved by employing the double CCRs.

In addition, an uncoated Fabry–Perot etalon with a thickness of 0.05 mm has been inserted into the resonator to adjust the wavelength of the Er:LuAG SLM laser. The SLM wavelength can be adjusted from 1649.2 nm to 1650.3 nm by changing the angle of the Fabry–Perot etalon at the pump power of 27.3 W. The SLM powers under the different output wavelengths have been shown in Table 1. The maximum output power is 1.61 W at the wavelength of 1649.6 nm, and the minimum output power is 0.50 W at the wavelength of 1650.1 nm.

Table 1. The Relationship between the SLM Wavelength and the Output Power.

Wavelength (nm)	Output Power (W)
1649.2	1.59
1649.4	1.09
1649.6	1.61
1650.1	0.50
1650.3	0.66

4. Er:LuAG Single-Pass Amplifier

To further increase the Er:LuAG SLM power, we designed a single-pass laser amplifier at 1649.6 nm. The experimental diagram of the SLM Er:LuAG MOPA laser is shown in Fig. 1. The size of 1.7 mm × 5.5 mm × 50 mm, 0.75% (atomic fraction) doped Er:LuAG1 crystal is used in the amplifier and installed in a water-cooled copper microchannel radiator with a temperature of 288 K. The Er:LuAG SLM laser and the residual pump light are focused by the f5 lens (160 mm) and the f4 lens (80 mm) to realize the spot matching. The beam radii are calculated to be 130 μm and 140 μm in the center of Er:LuAG-1, respectively. M3 and M4 are both 45° plane mirrors coated for high reflectivity at 1.5 μm and high transmission at 1.6 μm. M2 is a 1.6 μm polarizer coated with s-polarized high reflectivity and p-polarized high transmission. In addition, to compare the amplifier gain at different injection powers, a half-wave plate is used to adjust the power of the SLM oscillator. At a fixed total pump power of 27.3 W, all the residual 1.5 μm laser has been injected into the Er:LuAG-1. Then, the output power of the seed light is gradually increased, controlled by the half-wave plate in Fig. 1.

In Fig. 7, the amplified power and gain are shown as a function of the seed power. With the increase of the injected seed power, the gain of the Er:LuAG amplifier decreases, and the output power increases gradually. The output power is a maximum of 2.32 W at the injected power of 1.61 W, corresponding to the optical gain of 1.59 dB. The slope and the optical-to-optical efficiencies are 23.2% and 8.5%, respectively. The slope efficiency has been improved by 8% compared with the slope efficiency of the Er:LuAG SLM oscillator. Additionally, when the injection power is reduced to 295 mW, the output power is amplified to 532 mW, and the corresponding gain of 2.56 dB is obtained. The laser still operates in the SLM, tested by scanning Fabry–Perot interferometer at the amplification power of 2.32 W. As shown in Fig. 8(a), the measured beam quality factors M^2 are 1.23 and 1.25 along the horizontal (x) and vertical (y) directions, respectively. In Fig. 8(b), we have measured the power stability within 30 minutes and calculated a 5.27% power instability.

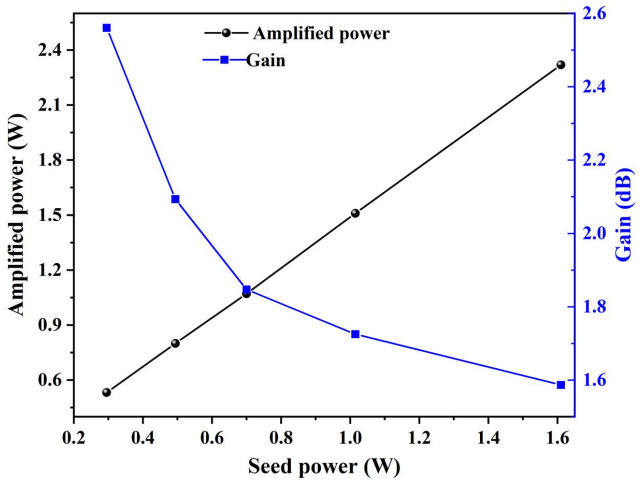

Fig. 7. The gain and the amplified power versus the seed power.

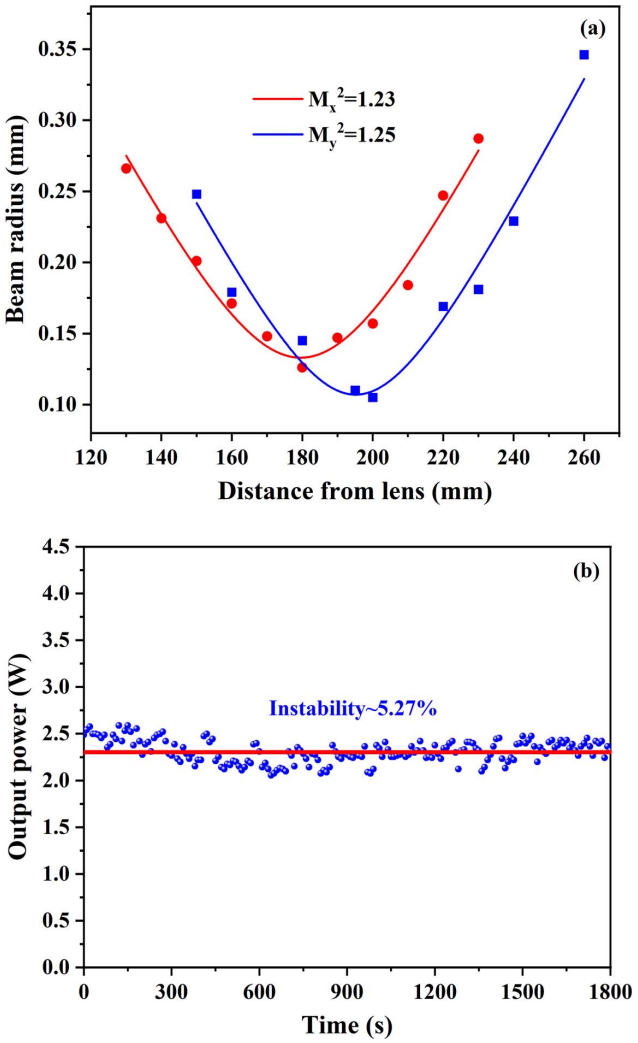

Fig. 8. Laser properties of the Er:LuAG single-pass amplifier. (a) Beam qualities M^2 of the 2.32 W SLM laser. (b) The power stability within 30 minutes.

5. Conclusions

In summary, we have built an SLM Er:LuAG laser with double CCRs and the MOPA system. The Er:LuAG SLM oscillator based on the Faraday effect achieves an output power of 1.61 W with a slope efficiency of 15.18%. The wavelength tunable range is 1649.2–1650.3 nm. Furthermore, by using the residual (non-absorbed) pump power of the Er:LuAG SLM oscillator, the single-pass amplifier obtains the maximum output power of 2.32 W, corresponding to the total slope efficiency, which has increased to 23.2%. Furthermore, the maximum gain is 2.56 dB with the SLM output power of 295 mW. Experimental results indicate that the unidirectional operation ring cavity based on the Faraday effect in the double CCRs structure is an effective way to produce the high-power, high-stability 1.6 μm Er:LuAG SLM laser.

Acknowledgements

This work was supported by the National Natural Science Foundation of China (Nos. U20A20214 and 62275067).

References

1. A. I. R. Malm, R. Hartman, and R. C. Stoneman, "High-power eyesafe YAG lasers for coherent laser radar," in *Advanced Solid-State Photonics* (Optica Publishing Group, 2004), paper WA6.
2. K. Mizutani, S. Ishii, M. Aoki, *et al.*, "2 μm Doppler wind lidar with a Tm: fiber-laser-pumped Ho:YLF laser," Opt. Lett. **43**, 202 (2018).
3. S. W. Henderson and S. M. Hannon, "Advanced coherent lidar system for wind measurements," Proc. SPIE **5887**, 58870I (2005).
4. J. Buck, A. Malm, A. Zakel, *et al.*, "High-resolution 3D coherent laser radar imaging," Proc. SPIE **6550**, 655002 (2007).
5. B. Q. Yao, T. Y. Dai, Y. Deng, *et al.*, "Tunable single-longitudinal-mode Er: YAG laser using a twisted-mode technique at 1.6 μm," Laser Phys. Lett. **12**, 025004 (2015).
6. D.-W. Chen, P. M. Belden, T. S. Rose, *et al.*, "Narrowband Er:YAG nonplanar ring oscillator at 1645 nm," Opt. Lett. **36**, 1197 (2011).
7. S. Huang, C. Chen, K. Wang, *et al.*, "High efficiency tunable unidirectional single-longitudinal-mode Er:YAG ring laser based on an acousto-optic modulator," Opt. Express **29**, 6445 (2021).
8. J. Fan, J. Wu, C. Jiang, *et al.*, "A single-longitudinal-mode Er:YAG laser and MOPA system based on the Faraday effect," Infrared Phys. Technol. **133**, 104789 (2023).
9. Y. Shi, C. Q. Gao, S. H. Li, *et al.*, "Fiber-bulk hybrid Er:YAG laser with single frequency output at the wavelengths of 1620 nm and 1656 nm," Laser Phys. Lett. **16**, 075001 (2019).
10. L. N. Zhu, C. Q. Gao, R. Wang, *et al.*, "Resonantly pumped 1.645 μm single longitudinal mode Er:YAG laser with intracavity etalons," Appl. Opt. **51**, 1616 (2012).
11. Y. Deng, B.-Q. Yao, J.-Y. L. Ju, *et al.*, "A diode-pumped 1617 nm single longitudinal mode Er:YAG laser with intra-cavity etalons," Chin. Phys. Lett. **31**, 074202 (2014).
12. T.-Y. Dai, X.-G. Xu, L. Ju, *et al.*, "Continuous-wave and actively Q-switched diode-pumped Er:LuAG ring laser at 1650 nm," Chin. Phys. Lett. **33**, 064207 (2016).
13. S. D. Setzler, K. J. Snell, T. M. Pollak, *et al.*, "5 W repetitively Q-switched Er: LuAG laser resonantly pumped by an erbium fiber laser," Opt. Lett. **28**, 1787 (2003).
14. S. Y. Zhang, L. Guo, M. Q. Fan, *et al.*, "Passively Q-switched Er:LuAG laser at 1.65 μm using MoS_2 and WS_2 saturable absorbers," IEEE Photon. J. **9**, 1502707 (2017).
15. T. Dai, J. Wu, Z. Zhang, *et al.*, "Diode-end-pumped single-longitudinal-mode Er:LuAG laser with intracavity etalons at 1.6 μm," Appl. Opt. **54**, 9500 (2015).
16. Z. Zhang and Y. Ju, "Theoretical and experimental studies of output coupling ratio tunable double-corner-cube-retroreflector ring cavity," J. Opt. Soc. Am. B **38**, 2847 (2021).
17. J. A. Macken and R. T. Salvage, "Alignment-insensitive resonators using focusing corner cubes," Proc. SPIE **1224**, 386 (1990).
18. S. E. Segre and V. Zanza, "Mueller calculus of polarization change in the cube-corner retroreflector," J. Opt. Soc. Am. A **20**, 1804 (2003).
19. Q. Sheng, M. Wang, H. Ma, *et al.*, "Continuous-wave long-distributed-cavity laser using cat-eye retroreflectors," Opt. Express **29**, 34269 (2021).
20. Q. Sheng, A. Wang, M. Wang, *et al.*, "Enhancing the field of view of a distributed-cavity laser incorporating cat-eye optics by compensating the field-curvature," Opt. Laser. Technol. **151**, 108011 (2022).
21. D. Wright, P. Greve, J. Fleischer, *et al.*, "Laser beam width, divergence and beam propagation factor—an international standardization approach," Opt. Quantum Electron. **24**, S993 (1992).
22. M. A. Acharekar, "Derivation of internal incidence angles and coordinate transformations between internal reflections for corner reflectors at normal incidence," Opt. Eng. **23**, 235669 (1984).
23. D. Xie and L. Zhu, "Microstrip leaky-wave antennas with nonuniform periodical loading of shorting pins for enhanced frequency sensitivity," IEEE Trans. Antennas Propag. **66**, 3337 (2018).